Journal of Hazardous Materials 436 (2022) 129270

Contents lists available at ScienceDirect

Journal of Hazardous Materials

journal homepage: www.elsevier.com/locate/jhazmat

Research Paper

Facile synthesis of sodium lignosulfonate/polyethyleneimine/sodium alginate beads with ultra-high adsorption capacity for Cr(VI) removal from water

Yimin Huang [a], Bing Wang [b], Jiapei Lv [c], Yingnan He [a], Hucai Zhang [a], Wenyan Li [d], Yongtao Li [d], Thomas Wågberg [e], Guangzhi Hu [a,e,*]

[a] Institute for Ecological Research and Pollution Control of Plateau Lakes, School of Ecology and Environmental Science, Yunnan University, Kunming 650504, China
[b] College of Resources and Environmental Engineering, Guizhou University, Guiyang, Guizhou 550025, China
[c] State Key Laboratory of Environmental Criteria and Risk Assessment, Chinese Research Academy of Environmental Sciences, Beijing 100012, China
[d] Joint Institute for Environmental Research and Education, College of resources and environment, South China Agricultural University, Guangzhou 510642, China
[e] Department of Physics, Umeå University, Umeå 901 87, Sweden

HIGHLIGHTS

- Simple cross-linking synthetic strategy was designed for beads synthesis.
- Maximum adsorption capacity of the SL/PEI/SA for Cr (VI) was up 2015.3 mg g^{-1}.
- High removal efficiency for Cr(VI) in wastewater environments.
- The presence of sodium humate contributed to the Cr(VI) removal rate.
- Removal mechanism contains both electrostatic adsorption and reduction.

GRAPHICAL ABSTRACT

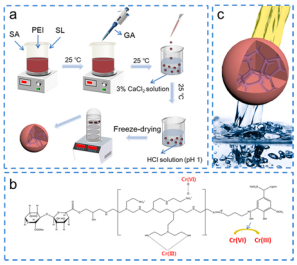

ARTICLE INFO

Editor: Sungjun Bae

Keywords:
Cr(VI) removal
Electroplating wastewater
Dynamic adsorption
Redox

ABSTRACT

Chromium (VI) is a widely occurring toxic heavy metal ion in industrial wastewater that seriously impacts the environment. In this study, we used environmentally friendly sodium lignosulfonate (SL), polyethyleneimine (PEI), and sodium alginate (SA) to synthesize SL/PEI/SA beads by employing a simple crosslinking method with to develop a novel absorbent with excellent adsorption capacity and practical application in wastewater treatment. We studied the adsorption performance of SL/PEI/SA through batch adsorption and continuous dynamic adsorption experiments. SL/PEI/SA has ultra-high adsorption capacity (2500 mg·g^{-1}) at 25 ℃, which is much higher than that of existing adsorbents. Humic acids and coexisting anions commonly found in wastewater have minimal effect on the adsorption performance of SL/PEI/SA. In the column system, 1 g SL/PEI/SA can treat 8.1 L secondary electroplating wastewater at a flow rate of 0.5 mLmin^{-1}, thereby enabling the concentration of Cr(VI) in secondary electroplating wastewater to meet the discharge standard (< 0.2 mg·L^{-1}). It is worth noting that the concentration of competitive ions in secondary electroplating wastewater is more than 500 times higher than that of Cr(VI). These results demonstrate that the novel SL/PEI/SA beads can be effectively applied in the removal of Cr(VI) in wastewater.

* Corresponding author at: Institute for Ecological Research and Pollution Control of Plateau Lakes, School of Ecology and Environmental Science, Yunnan University, Kunming 650504, China.
E-mail address: guangzhihu@ynu.edu.cn (G. Hu).

https://doi.org/10.1016/j.jhazmat.2022.129270
Received 4 February 2022; Received in revised form 18 May 2022; Accepted 29 May 2022
Available online 2 June 2022

1. Introduction

Chromium (Cr) is a heavy metal that is widely used in industrial applications, including textile mills, electroplating plants, wood mills, and tanneries (X. Wang et al., 2020; Y. Wang et al., 2020). Owing to its high solubility and bioaccumulation, Cr is often detected in natural water sources (Liu et al., 2019). Cr exists in two main oxidation states: Cr (VI) and Cr(III) (Yang et al., 2022) with the former being non-biodegradable and 500 times more toxic than the latter (Chen et al., 2016). Therefore, Cr(VI) has been flagged as an extremely dangerous pollutant by the US Environmental Protection Agency (Liu et al., 2019), while the International Agency for Research on Cancer (IARC) has classified it as a group-1 human carcinogen (Su et al., 2021). Therefore, reducing the concentration of Cr (VI) in industrial wastewater to an acceptable level is crucial for safeguarding environmental and human health (Guo et al., 2018).

Among the applied strategies for mitigating Cr(VI) pollution, adsorption is considered one of the most effective approaches because of its low cost, ease of operation, and ability to remove low-concentration pollutants (Huang et al., 2018b; Zhao et al., 2017). To prevent adsorbent induced secondary pollution in water environments, certain environmentally compatible adsorbents for Cr(VI) removal have been developed, such as those based on activated carbon (Nasseh et al., 2021), zeolite (Zhang et al., 2018), montmorillonite (Wang et al., 2016), biochar (Lian et al., 2019), and cellulose (Liao et al., 2020). However, their adsorption capacity and Cr(VI) removal efficiency are yet to reach satisfactory levels (Fang et al., 2021). Therefore, the development of a new adsorbent featuring environmental compatibility, ultra-high adsorption capacity, and potent Cr(VI) removal efficiency from water environments is of paramount importance.

Sodium alginate (SA) is a non-toxic, biocompatible, renewable and low-cost polysaccharide derived from sea algae (Feng et al., 2021). It contains abundant carboxylate groups (COOH), which can chelate with metal ions to form a complex "egg-box" structure (Y. Yan et al., 2017; Y.-Z. Yan et al., 2017), and can be used as an adsorbent to remove Cr(VI) from water environments (Wang et al., 2019). In addition, SA can yield a hydrogel under the action of calcium ions, which facilitates the recovery of the adsorbent from aqueous solutions (Feng et al., 2021). These excellent characteristics of SA make it get considerable attention in the field of wastewater treatment (Jiao et al., 2020). However, because of the lack of reducibility, the adsorption capacity of pure SA gel for Cr(VI) is unsatisfactory. In addition, SA has low mechanical strength and is fragile, which affects its reusability and large-scale application in industry. Accordingly, the introduction of additional components into the SA hydrogel for improving its adsorption and mechanical features has been proposed (Feng et al., 2021; Jiao et al., 2020).

Polyethyleneimine (PEI), a polyamine containing multiple amine groups, has been widely used for adsorbent modification because of its strong ability to chelate heavy metal ions (Sun et al., 2016). In recent years, the introduction of PEI into SA gels to improve the mechanical strength and Cr(VI) adsorption capacity of SA gel beads has been reported. For example, Yan et al. coated PEI on the surface of SA gel beads by cross-linking reaction, which not only improved the mechanical properties of SA gel beads, but also increased the maximum adsorption capacity of SA gel beads to 431.6 $mg{\cdot}g^{-1}$ (Yan et al., 2017). Feng et al. modified SA by crosslinking reaction with MXene and PEI. The double network structure that formed following the modification of SA by PEI significantly enhanced the mechanical strength of SA gel. In addition, the abundant active groups of PEI and the in-situ reduction ability of MXene dramatically improved the adsorption capacity of SA gel for Cr (VI) to 538.97 $mg{\cdot}g^{-1}$. However, the adsorption capacity of MXene/-PEI/SA for Cr (VI) was significantly inhibited by high concentration of competitive anions (Feng et al., 2021). Considering the complex components in industrial wastewater, it is necessary to introduce some new components, which will greatly enhance the adsorption and removal ability of SA gel beads for Cr(VI) in wastewater.

SL has great potential to improve the adsorption capacity of SA gel beads to Cr(VI). SL is an inevitable by-product of paper industry, and has excellent characteristics similar to SA, such as environmental friendliness, low cost, and rich functional groups (hydroxyl and sulfonic acid) (Gao et al., 2018; Liu et al., 2020; Yang et al., 2020). These characteristics render it as a potential candidate for enhancing the adsorption capacity of the absorbents, which can remove Cr(VI). For example, graphene modified by SL shows a high adsorption capacity of 1743.9 $mg{\cdot}g^{-1}$ for Cr(VI), which verifies the advantage of SL modified adsorbent for Cr(VI) removal (Sun et al., 2021). At present, there has been a research repored that SL can be crosslinked with PEI through glutaraldehyde (Xie et al., 2020), so SL has the potential to improve the adsorption performance of SA gel beads through crosslinking reaction with PEI and to synthesize an adsorbent with ultra-high adsorption capacity for Cr(VI) removal from wastewater.

In this study, we synthesized SA gel beads modified by PEI and SL (SL/PEI/SA) at 25 ℃ through simple crosslinking reactions. The main contributions of this study are summarized as follows: (1) The optimal adsorption parameters/capacity of the SL/PEI/SA gel beads were determined through batch adsorption experiments. Concurrently, the adsorption data were fitted using kinetic and thermodynamic models to study the main adsorption mechanism. (2) The adsorption-desorption experiments were run 10 times to understand the regenerative adsorption capacity of the SL/PEI/SA beads. (3) The effects of competitive ions and humic acid on SL/PEI/SA adsorption were investigated. (4) The ability of SL/PEI/SA to treat wastewater was investigated through batch adsorption and continuous dynamic adsorption experiments.

2. Materials and Methods

2.1. Materials and reagents

SA, SL, and PEI were purchased from Shanghai Aladdin Bio-Chem Technology Co., LTD. Glutaraldehyde (GA, 25 %) was purchased from Tianjin Kemio Chemical Reagent Co., LTD. Potassium dichromate (KCD) was purchased from Macklin. All reagents were used directly without further purification. The solution was prepared using ultrapure water (18.25 MΩ·cm) as the solvent.

2.2. Synthesis of adsorbents

The preparation processes of SL/PEI/SA are shown in Fig. S1. The specific process is as follows: 0.2 g of SA, 0.2 g of PEI, and 0.2 g of SL are added to a 50 mL beaker containing 15 mL of water and was stirred at 25 ℃. After 12 h, 0.7 mL of glutaraldehyde was added to the above beaker and stirred continuously for 5 h at 25 ℃ Subsequently, the solution was dropped into a 3 % of $CaCl_2$ solution to form beads. After allowing this solution to stand for 12 h, the beads were filtered and washed three times with water, and subsequently suspended in an aqueous solution with a pH of 1 for 24 h. Finally, the beads were repeatedly washed with water and freeze-dried to obtain SL/PEI/SA beads. Concurrently, SA, SL/SA, PEI/SA, and SL/PEI/SA_1 were synthesized according to the aforementioned steps. The difference between SL/PEI/SA_1 and SL/PEI/ SA is that glutaraldehyde was not added in the process of synthesizing SL/PEI/SA_1.

2.3. Adsorbent characterization

Fourier transform infrared (FTIR) spectroscopy was used to obtain information on the functional groups of the adsorbent (Bruker MPA and Tensor 27, Germany). X-ray photoelectron spectroscopy (XPS) was used to analyze the chemical composition of the components on the adsorbent surface (Thermo Fisher K-Alpha+, USA). Scanning electron microscopy (SEM) was used to observe the morphology and particle size distribution of the adsorbent (Zeiss Sigma300, Germany). The specific surface area, pore volume, and pore size distribution of the adsorbent were obtained

using a special analyzer (TriStar II 3flex, USA).

2.4. Adsorption experiments

A Cr(VI) solution with an initial concentration of (50–1400) mg·L^{-1} was prepared using potassium dichromate. The adsorbent and Cr(VI) solution were mixed at a solid-to-liquid ratio of 1:10–1:1 (g:L) and shaken at 150 rpm. After the adsorption process reached equilibrium, the filtrate was filtered through a 0.45 μm filter. The Cr(VI) concentration in the filtrate was measured using an ultraviolet spectrophotometer (Thermoscientific, Genesys 50) and inductively coupled plasma emission spectrometer (ICP-OES, Aglient 5110).

2.5. Desorption experiment

The regeneration ability of an adsorbent is an important index of its practical application potential. In this study, the SL/PEI/SA beads were tested for 10 adsorption-desorption experimental cycles. Within 6 h, the SL/PEI/SA beads reached more than 80 % of their maximum adsorption capacity. Considering the time, 30 mg of SL/PEI/SA was added to a Cr (VI) solution with a concentration of 400 mg·L^{-1} and was shaken for 6 h. Subsequently, SL/PEI/SA (separated from the Cr(VI) solution) was added to 30 mL of a NaOH solution with a concentration of 0.05 M and was allowed to desorb for 2 h. Finally, the SL/PEI/SA beads were filtered and cleaned with water before each adsorption session. The final process was repeated 10 times.

2.6. Dynamic adsorption experiment

The dynamic adsorption experiment was carried out in a chromatographic column with an inner diameter of 1.7 cm and a height of 20 cm. The weight of the SL/PEI/SA gel beads filled in the chromatographic column was 1.0 g, and the filling bed height was 10 cm. The dynamic adsorption experiment can be divided into two parts as described below.

(1) The Cr(VI) solution with an initial concentration of 100 mg·L^{-1} was controlled by a peristaltic pump to enter the chromatographic column from top to bottom at a flow rate of 1.5 mL·min^{-1}. The Cr(VI) solution was collected at different times until its concentration reached 90 % of the initial concentration (exhaustion point).

(2) The secondary electroplating wastewater was passed through the chromatographic column at the rate of 0.5 mL·min^{-1}, and the filtrate was continuously collected until the concentration of Cr(VI) in the filtrate reached 0.2 mg·L^{-1}.

2.7. Applicability of SL/PEI/SA to wastewater treatment

To investigate the ability of SL/PEI/SA to remove Cr(VI) in electroplating wastewater that contains a high concentration of Cr(VI), an adsorption experiment was carried out using untreated electroplating wastewater collected from the Jiangyan Longgou electroplating plant (Taizhou City, Jiangsu Province, China). SL/PEI/SA gel beads were added to a 100 mL conical flask containing 30 mL of electroplating wastewater, and the changes in the components of the wastewater before and after adsorption were measured at the adsorption equilibrium point.

3. Results and discussion

3.1. Characterization of SL/PEI/SA

3.1.1. SEM analysis

The micromorphology and structure of the adsorbent are important factors affecting its adsorption performance. Fig. 1 shows the micromorphology of the SL/PEI/SA gel beads investigated via SEM. The beads mainly comprised a three-dimensional (3D) porous structure with many circular and oval pores (Fig. 1a,b,c). These 3D pores, which were constructed by the cross-linking between SA, PEI, and SL, can rapidly penetrate water and Cr(VI) molecules (Fig. 1). This process can significantly promote the reaction rate between the Cr(VI) molecules and the SL/PEI/SA active sites (Q. Wang et al., 2021; X. Wang et al., 2021). Furthermore, the presence of SA induced the formation of many irregular macro-porous structures in the cross-sectional regions of the SL/PEI/SA beads (Zhang et al., 2019). After adsorbing Cr(VI) (Fig. 1a), the pores on the SL/PEI/SA beads were blocked (Fig. 1e, f). The energy-dispersive X-ray spectroscopy (EDS) results confirmed that the adsorbed Cr(VI) species led to pore caking or blockage on the gel beads (Fig. 1g).

3.1.2. Brunauer–Emmett–Teller (BET) analysis

The pore size distribution results for the SL/PEI/SA gel beads before and after Cr(VI) adsorption are shown in Fig. 2a and b, respectively. Before Cr(VI) adsorption (Fig. 2a), the N_2 adsorption–desorption isotherm curve showed evident hysteretic loops. Furthermore, the pore size distribution in Fig. 2a shows that the pores of the SL/PEI/SA beads fluctuated between 400 and 1000 nm in size, while the average pore size was 13.5 nm, suggesting that SL/PEI/SA is mainly a mesoporous structure. After Cr(VI) adsorption (Fig. 2b), the pore size of the SL/PEI/SA beads ranged between 50 nm and 200 nm, and the average pore size was reduced to 12.1 nm, which is caused by the adsorbed Cr(VI) that occupies the pores. (as shown in SEM Fig. 1f).

3.1.3. FTIR Analysis

To further investigate the reaction mechanism underlying the crosslinking between the SA, PEI, and SL molecules, the functional groups of the SL/PEI/SA$_1$ and SL/PEI/SA beads were compared (Fig. 2c). In the SL/PEI/SA$_1$, a wide peak appeared at 3400–3500 cm^{-1}, which was attributed to the –OH groups from SA and SL (Feng et al., 2021; Zhang et al., 2021). The peak at 2929.3 cm^{-1} was attributed to the –CH_2 groups from PEI and SL (X. Wang et al., 2021; Q. Wang et al., 2021; Zhang et al., 2021). In addition, two distinct peaks at 1740 cm^{-1} and 1244.1 cm^{-1} were respectively assigned to the carbonyl stretch of –COOH (Huang et al., 2018c; Zhang et al., 2019) and active –OH groups in SA (Zhao et al., 2021). Moreover, the characteristic peaks at 1042 cm^{-1}, 650 cm^{-1}, and 536 cm^{-1} were attributed to the –SO_3H groups from LS (Q. Wang et al., 2021; X. Wang et al., 2021). After adding the crosslinking agent, the peak at 3415 cm^{-1} representing the –COOH groups in SA disappeared, and the peak from SL/PEI/SA$_1$ at 3415 cm^{-1} shifted to 3412 cm^{-1}. This phenomenon stemmed from the reaction between glutaraldehyde and the –COOH groups of SA (Fig. 7) (Feng et al., 2021). In addition, the peak of the –CH_2 group of SL/PEI/SA$_1$ at 2929.3 cm^{-1} was significantly weakened, and a new peak appeared at 1660 cm^{-1}, which corresponded to the C═N bond formed by the cross-linking of SA/PEI/SL and GA (Xie et al., 2020; Xue et al., 2022). The changes in these characteristic peaks showed that SA, PEI, and SL were crosslinked by chemical reactions.

Notably, the peak of SL/PEI/SA$_1$ representing the aromatic lignin ring at 1590 cm^{-1} still existed after the crosslinking reaction, suggesting that the original lignin structure underwent minimal changes (Sun et al., 2021). The comparison between PEI/SA and SL/PEI/SA showed that after SL addition, the PEI/SA peak representing –OH at 3413.7 cm^{-1} shifted to 3412.9 cm^{-1} (Feng et al., 2021). Moreover, the peak intensity increased significantly, indicating that the addition of SL increased the content of –OH groups.

After the adsorption of Cr(VI), two new peaks appeared at 896.89 cm^{-1} and 545 cm^{-1}, representing Cr(VI)–O and N–Cr(VI), respectively (Feng et al., 2021; Zhang et al., 2020), which proved that Cr (VI) was successfully adsorbed by SL/PEI/SA. Meanwhile, the peaks representing –OH, amide I vibration, the bending vibration of C–H, and the stretching vibration of C–O–C shifted to 3412.53 cm^{-1}, 1617.5 cm^{-1}, 1384.06 cm^{-1}, and 1073.61 cm^{-1} (Chen et al., 2011; Feng et al., 2021; Wang et al., 2021), and the intensity of these four peaks decreased. The

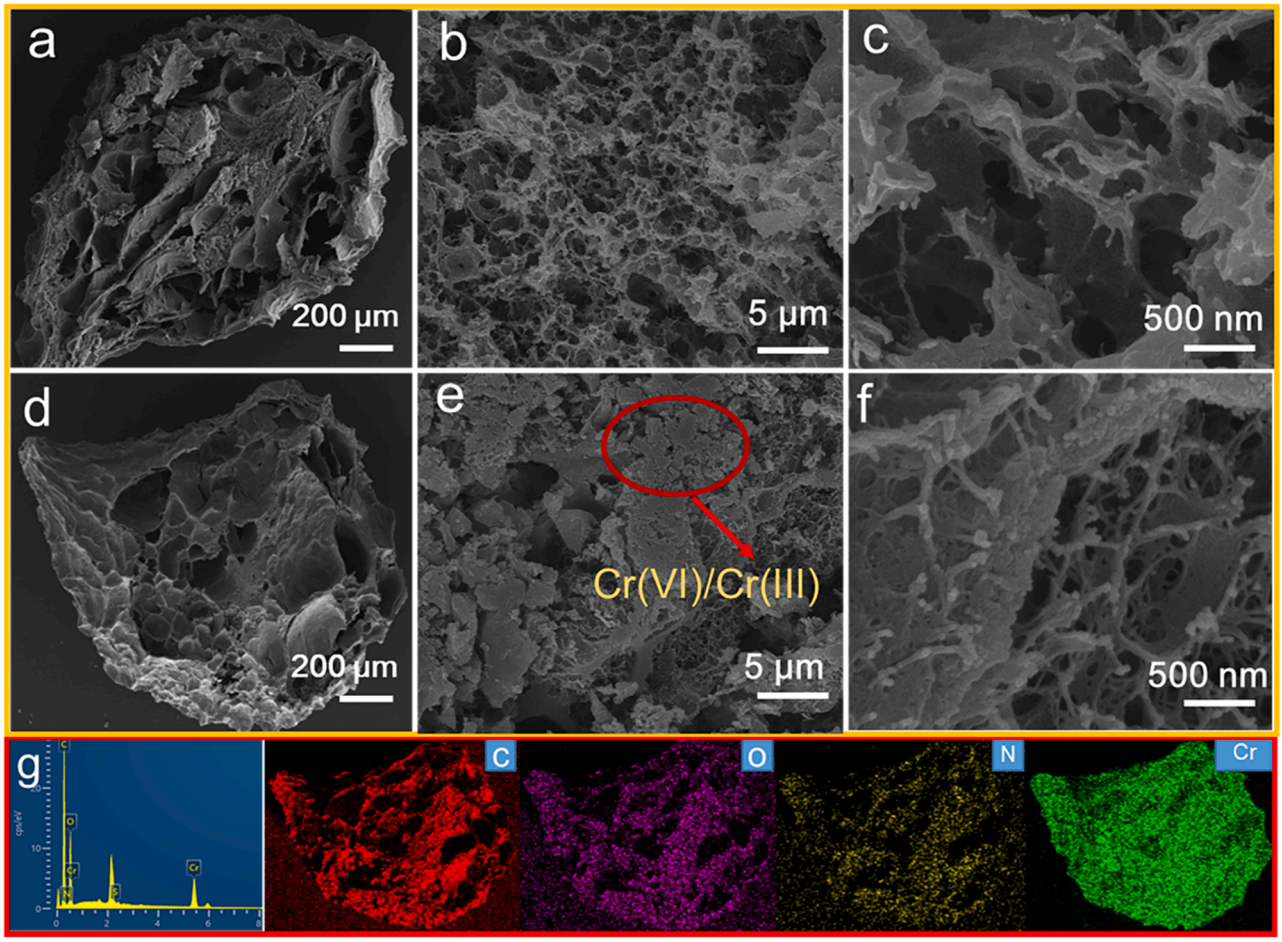

Fig. 1. SEM images of the SL/PEI/SA gel beads before (a, b, c) and after (d, e, f) Cr(VI) adsorption. (g) EDS elemental mapping of SL/PEI/SA gel beads after Cr (VI) adsorption.

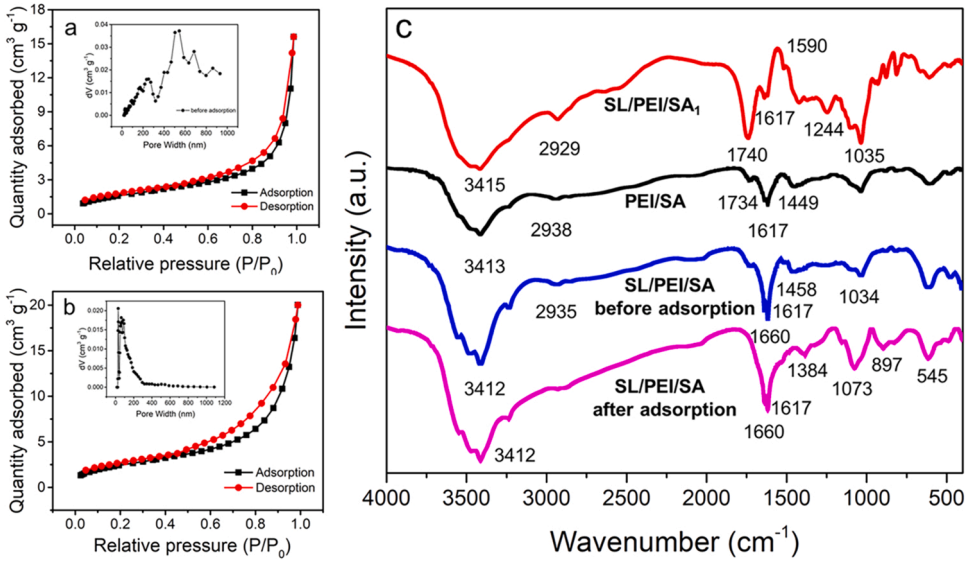

Fig. 2. N_2 adsorption–desorption isotherm curves and pore distribution of SA/PEI/SL gel beads (a) before and (b) after Cr(VI) adsorption. (c) FTIR spectra of SA/PEI, SA/PEI/SL_1 (without crosslinking agent), and SA/PEI/SL (with crosslinking agent) specimens.

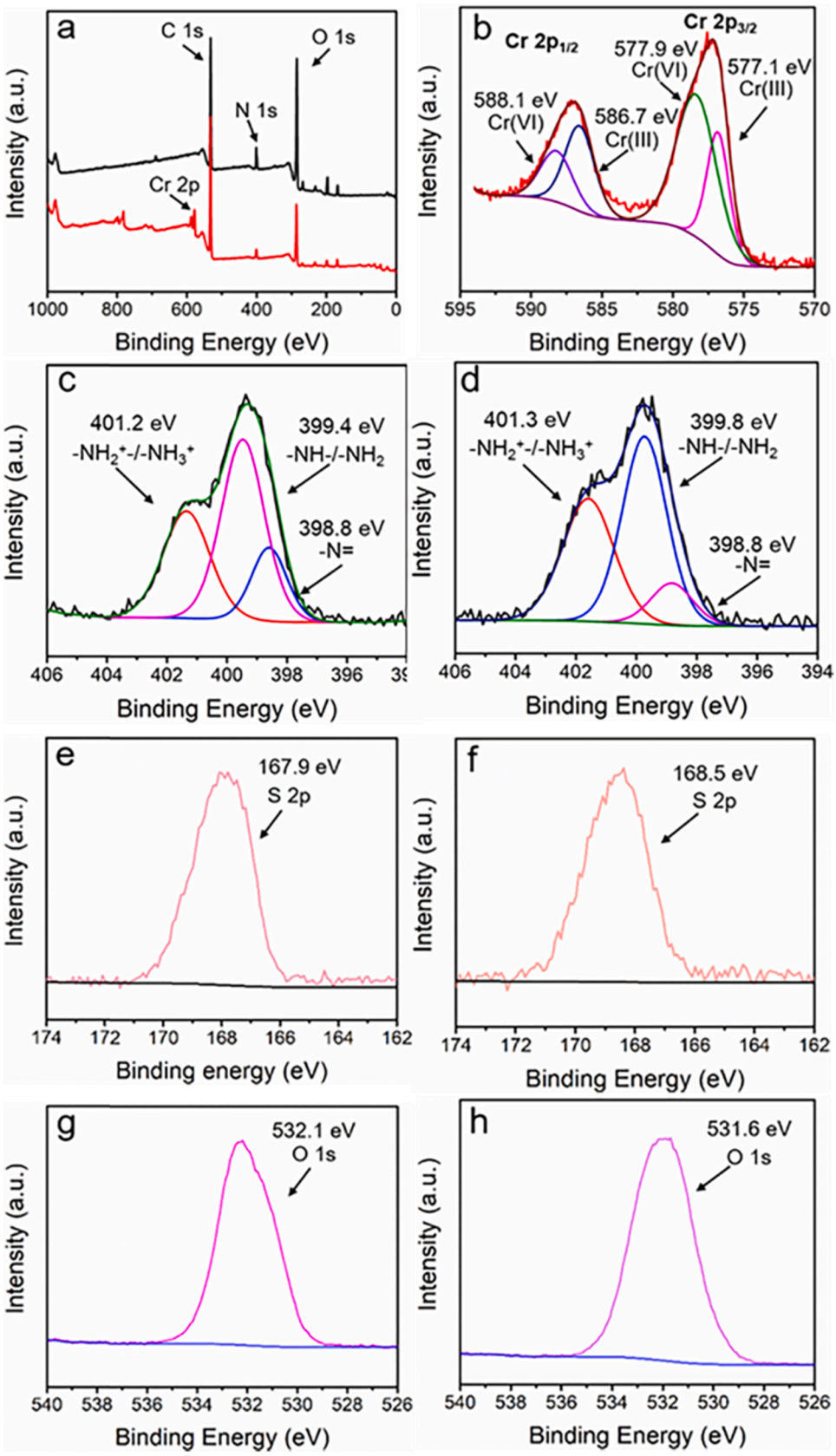

Fig. 3. XPS spectra before (left column) and after (right column) adsorption: (a) XPS spectra of SL/PEI/SA; (b) high-resolution XPS spectra of Cr 2p; (c, d) N 1 s XPS spectra; (e, f) S 2p XPS spectra; (g, h) O 1 s XPS spectra.

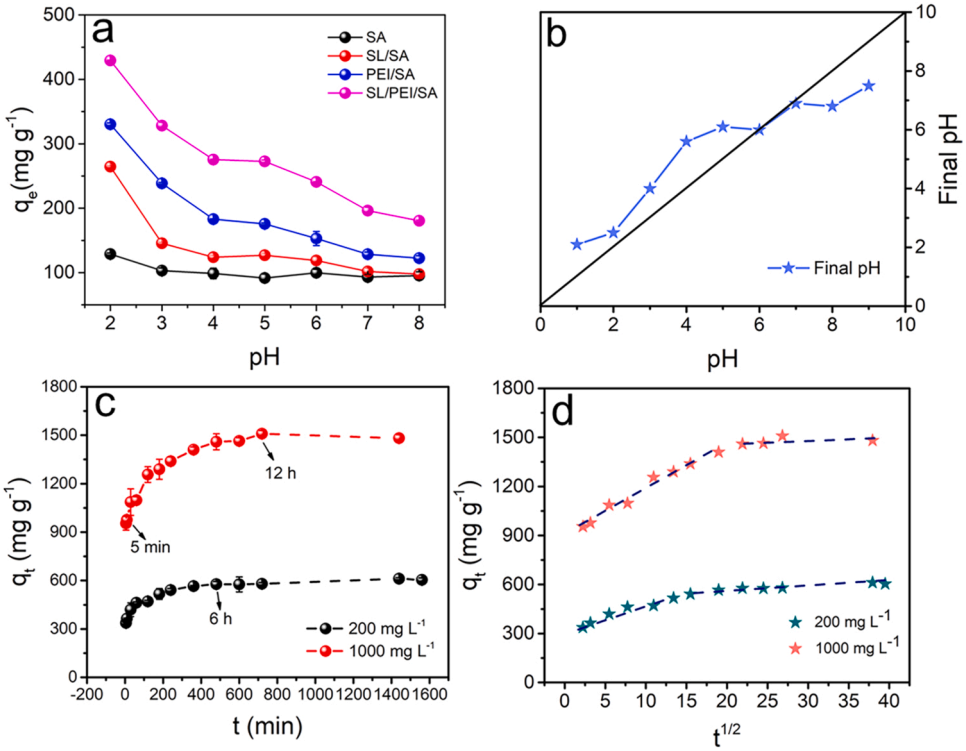

Fig. 4. (a) Changes in the Cr(VI) adsorption capacity of SA、SL/PEI、PEI/SA and SL/PEI/SA with different pH (Slid-liquid ratio: 0.45 g·L^{-1}; C_0: 200 mg.L^{-1}; T: 25 ℃; time: 24 h). (b) Change of final pH value after Cr(VI) adsorption with initial pH of solution. (c) Change of the adsorption capacity of SL/PEI/SA with time. (d) Intra-particle diffusion model for Cr(VI) adsorption on SL/PEI/SA. (Slid-liquid ratio: 0.1 g·L^{-1}; C_0: 200 mg·L^{-1}; T: 25 ℃; time: 24 h).

C═H/C–H stretching vibration peaks at 2935.47 cm^{-1} and 2860 cm^{-1} also decreased significantly (Q. Wang et al., 2021; X. Wang et al., 2021), indicating that these functional groups were involved in the process of Cr(VI) adsorption (See formula 3).

3.1.4. *XPS analysis*

The XPS results showed that after adding SL, the S content of PEI/SA increased from 0 % to 2.4 %, indicating that SL was successfully loaded onto the SL/PEI/SA gel beads (Table S1). Meanwhile, the O content increased from 22.2 % to 24.0 %, indicating that the addition of SL increased the number of oxygen-containing functional groups, such as –OH. In the high-resolution Cr 2p XPS spectrum (Fig. 3b), the peaks of Cr 2 $P_{3/2}$ and Cr $2p_{1/2}$ can be clearly observed. The peaks at 577.9 eV, 588.1 eV and 577.1 eV, 586.7 eV represent Cr(VI) and Cr(III), respectively (Fang et al., 2021). The presence of Cr(III) on the SL/PEI/SA bead surface indicated the reduction of Cr(VI) to Cr(III) during the adsorption process.

Fig. 3c and d show the high-resolution N 1 s spectra before and after SL/PEI/SA adsorption, respectively. The peaks of SL/PEI/SA at 401.1 eV, 399.1 eV, and 398.4 eV correspond to the protonated amine (–N = $^+$), amine (–NH–/–NH_2), and imine (–N =) groups, respectively (Bao et al., 2020; Zhang et al., 2019). After Cr(VI) adsorption, the binding energies of the three peaks shifted to 401.3 eV, 399.8 eV, and 398.8 eV, respectively, suggesting that the functional groups related to N were involved in the adsorption of Cr(VI). Functional groups related to N mainly participate in the adsorption of Cr(VI) in two ways: 1) The protonated amino group reacted with the negatively charged Cr(VI) species via electrostatic adsorption. 2) The amine to bind with the positively charged reduced Cr(III) species (Y.-Z. Yan et al., 2017; Y. Yan et al., 2017). In addition, it is worth noting that the peak attributed to –N = $^+$ appeared before the adsorption of Cr(VI) on the SL/PEI/SA surface. This behavior was theoretically attributed to the final preparation step of SL/PEI/SA, namely, immersion in an acidic solution, which resulted in the protonation of some amino groups on SL/PEI/SA.

After Cr(VI) adsorption, the peak representing O 1 s shifted from 167.9 eV to 168.5 eV (Fig. 3c and d). Meanwhile, the peak representing S 2p shifted from 532.1 eV to 531.6 eV (Fig. 3g and h), indicating that the O-related groups and sulfonic acid groups from lignin were also involved in the adsorption of Cr(VI) (Sun et al., 2021) (See formula 3 and 5).

3.2. *Effect of solution pH on Cr(VI) adsorption*

The pH of the solution can affect the electrical charges on the surface of the adsorbent and the existing form of Cr(VI) in the solution, thereby affecting the adsorption capacity of the adsorbent for Cr(VI). Therefore, the effect of pH on the Cr(VI) adsorption capacity of SL/PEI/SA was first investigated.

SL/PEI/SA was synthesized from SA, PEI, and SL components. To study the role of each component in the adsorption process, the adsorption capacities of SA, SL/SA, PEI/SA, and SL/PEI/SA for Cr(VI) at different pH were investigated. As shown in Fig. 4a, the adsorption capacity of SA, SL/SA, PEI/SA, and SL/PEI/SA increases gradually, indicating that SL and PEI can improve the adsorption capacity of SA. In addition, it is worth noting that SA and SL/SA were almost dissolved at pH 7, whereas PEI/SA and SL/PEI/SA beads remained stable at pH 8. This proves that PEI is an important component of cross-linking reaction with SA and SL, thereby making PEI/SA and SL/PEI/SA stable under neutral and alkaline conditions. Therefore, SL/PEI/SA was the adsorbent with the best adsorption efficiency and stability among the four adsorbents.

SL/PEI/SA had the largest adsorption capacity of Cr(VI) at pH 2 (429.3 mg·L^{-1}), and 44.1 % of Cr (VI) adsorbed on the surface of SL/PEI/SA was reduced to Cr (III). This was because a low pH value is conducive to the electrostatic adsorption and reduction of Cr (VI) (Song et al., 2019). As the pH of the solution increased from 2 to 8, the capacity of SL/PEI/SA for Cr(VI) adsorption decreased from 429.3 ± 4.2 mg.g^{-1} to 180.5 ± 1.3 mg g^{-1} (Fig. 4a). The reasons for the decrease in the

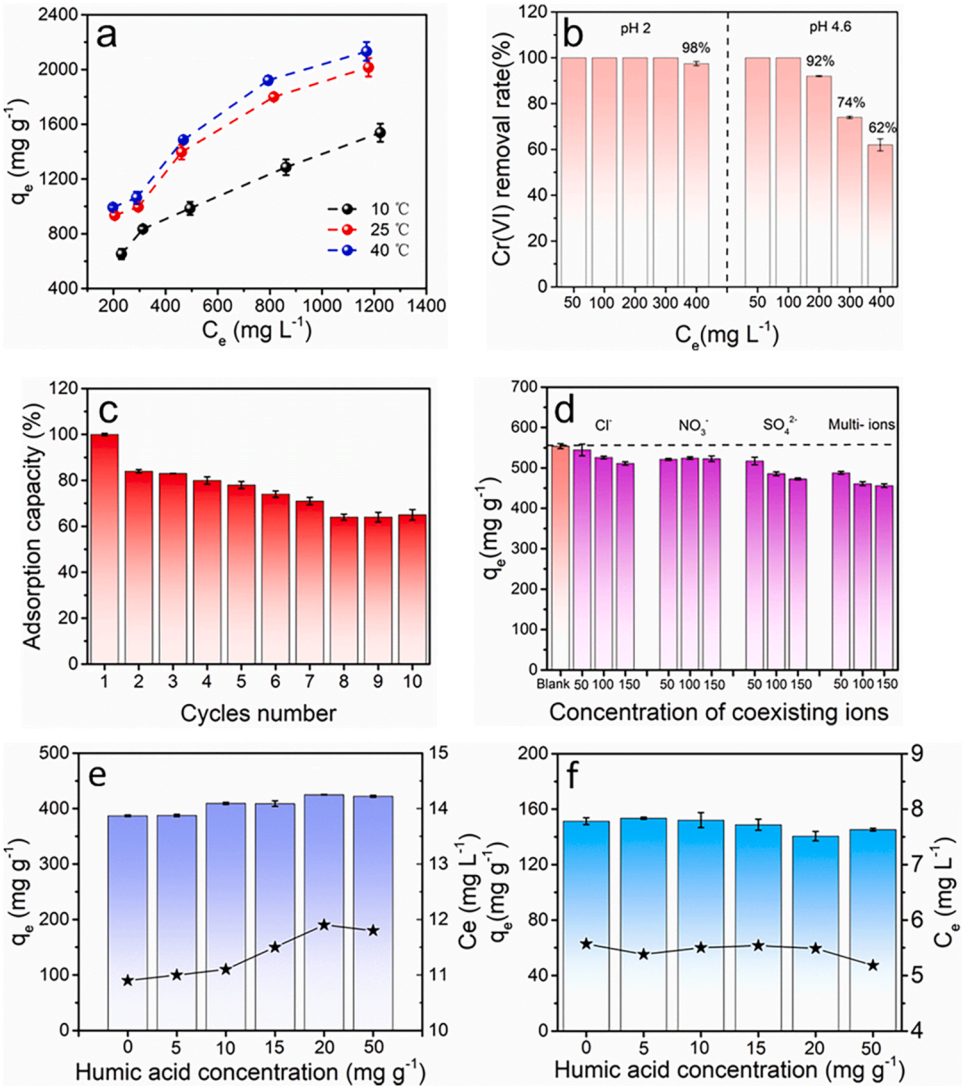

Fig. 5. (a) Adsorption capacity variation of SA/PEI/SL with the initial Cr(VI) concentration (C_0: 300 mg·L^{-1} to 1400 mg·L^{-1}; T: 10–40 ℃; pH: 2). (b) Changes in the removal rate of Cr(VI) by SA with initial concentration of Cr(VI) (C_0: 50 mg·L^{-1} to 400 mg·L^{-1}; T: 25 ℃; pH: 2 and 4.6). (c) Regeneration capacity of SA/PEI/SL (C_0: 400 mg·L^{-1}; T: 25 ℃; pH: 2). (d) Effect of coexisting ions concentration on SA/PEI/SL adsorption capacity (C_0: 100 mg·L^{-1}; T: 25 ℃; pH: 2). (e) Effect of concentration of humic acid (HA) on SA/PEI/SL adsorption capacity (C_0: 50 mg·L^{-1}; T: 25 ℃; pH: 2). The broken line represents the change of the concentration of Cr (III) in the filtrate with the concentration of HA. (f) Effect of concentration of humic acid (HA) on SA/PEI/SL adsorption capacity (C_0: 50 mg·L^{-1}; T: 25 ℃; pH: 7). The broken line represents the change of the concentration of Cr(III) in the filtrate with the concentration of HA.

adsorption capacity of SL/PEI/SA with the increase of pH are the follwoing: (1) The –OH group on SL/PEI/SA acts as an electron donor group and consumes H^+ in the solution, thus reducing a part of Cr(VI) in the solution to Cr (III) (See formula 3). As the pH increased from 2 to 8, the amount of SL/PEI/SA-reduced Cr(III) in the solution decreased from 147 mg·g^{-1} to 56 mg·g^{-1}, confirming that the reduced H^+ content in the solution negatively impacted the efficiency of SL/PEI/SA for Cr(VI) to Cr (III) reduction. (2) The point of zero charge (pHzpc) of SL/PEI/SA is 6, as identified by the pH drift method (Zhang et al., 2017). When the pH of the solution is less than 6, a large number of amino groups on the surface of SL/PEI/SA were protonated and positively charged (Fig. 4b) and therefore, could absorb additional Cr(VI) species (which were negatively charged). As the pH increased, the decreased number of protonated functional groups on the surface of SL/PEI/SA led to a weakening of its electrostatic adsorption effect on Cr(VI). (3) At pH 1–3, Cr (VI) in the solution mainly exists in the form of $HCrO_4$. With the increase in pH, CrO_4^{2-} gradually replaces $HCrO_4$. As the adsorption free energy of CrO_4^{2-} is higher than that of $HCrO_4$, CrO_4^{2-} is more difficult to be adsorbed than $HCrO_4^-$ with the same concentration. Consequently, resulting in a decrease in the adsorption capacity of SL/PEI/SA for Cr(VI) with the increase in pH. (Huang et al., 2018b). (4) The Cr(VI) species competed against an increased number of –OH radicals in the solution for the adsorption sites on SL/PEI/SA. As the pH of industrial wastewater with Cr(VI), such as electroplating wastewater, is typically in the range of approximately 2 ~ 3, we chose to investigate the adsorption performance of SL/PEI/SA at pH 2.

3.3. *Effect of adsorption time on Cr(VI) adsorption performance*

Fig. 4c shows the time curve of the adsorption amount of Cr(VI) by SL/PEI/SA. When the initial Cr(VI) concentration was 1000 mg·L^{-1}, the adsorption capacity of SL/PEI/SA for Cr(VI) reached as high as 954.5 ± 2 mg·g^{-1} (63 % of the total adsorption capacity) in the first 5 min and increased further to 93.5 % (1410.3 mg·g^{-1}) of the total adsorption capacity within 6 h. This indicated that a large number of active sites on SL/PEI/SA can notably accelerate the reaction with Cr(VI). The adsorption capacity of SL/PEI/SA in the first 5 min (954.5 ± 2 mg·g^{-1}) significantly exceeded the maximum adsorption capacity (q_m) of various reported excellent adsorbents, such as polydopamine (PDA)/PEI-modified $CaCO_3$ composites (524.7 mg·g^{-1}) (Yan et al., 2017), magnetic mesoporous polydopamine nanocomposites (574.71 mg·g^{-1}) (Yang et al., 2021), diethylenetriaminepentaacetic acid/thiourea-modified magnetic chitosan (321 mg·g^{-1}) (Liu et al., 2021), and Zn–MOF/chitosan composites (225 mg·g^{-1}) (Niu et al., 2021). For a lower Cr(VI) concentration (200 mg·L^{-1}), although the final equilibrium of Cr(VI) adsorption by SL/PEI/SA was reached at 24 h, SL/PEI/SA reached 59 % (337.2 ± mg·g^{-1}) and 94.4 % (578.0 ± 1 mg·g^{-1}) of the maximum adsorption capacity in 5 min and 8 h, respectively. These

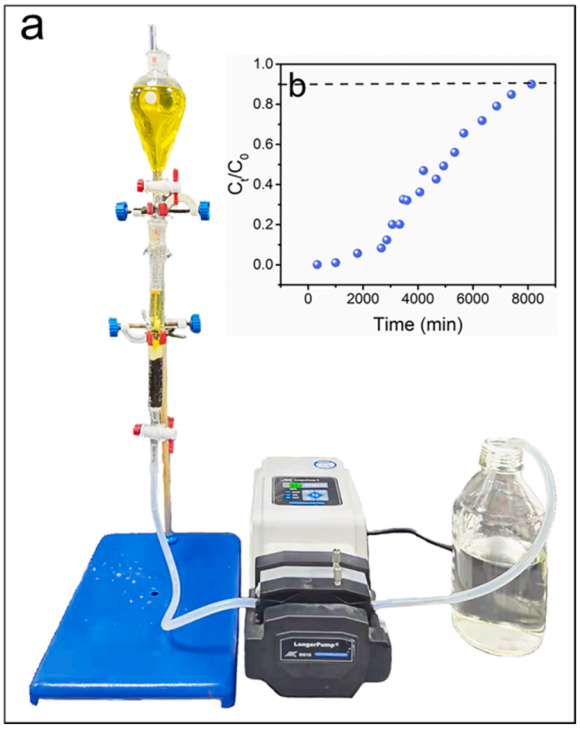

Fig. 6. (a) Column adsorption of SL/PEI/SA for Cr(VI). (b) Breakthrough curve of SL/PEI/SA to Cr(VI).

results confirm that SL/PEI/SA has the excellent ability to efficiently and rapidly remove of Cr (VI).

To further explore the mechanism of Cr(VI) removal by SL/PEI/SA and the limiting steps during the adsorption process, the kinetic data were fitted using first-order kinetics and second-order kinetics (as expressed by formula S1 and S2). The fitted parameters are listed in Table 1. The correlation coefficients (0.99 and 0.99) fitted using the second-order kinetics was higher than those fitted with the first-order kinetics (0.9 and 0.98), and the fitted equilibrium adsorption capacity of SL/PEI/SA was similar to the actual adsorption capacity of SL/PEI/SA, indicating that the second-order kinetics better described the adsorption process (Fig. S2). Therefore, the adsorption mechanism of Cr (VI) by SL/PEI/SA was inferred to mainly stem from chemical adsorption (Liang et al., 2019).

To understand the rate-limiting step, the Weber–Morris intra-particle diffusion model was employed to study the rate control process (as expressed by formula S3). The line fitted by the Weber–Morris intra-particle diffusion model did not pass through the origin (Fig. 4**d**), suggesting that inner particle diffusion was not the only rate-limiting step (Boparai et al., 2011). Moreover, the adsorption of Cr(VI) by SL/PEI/SA comprised two linear processes, indicating that the adsorption process included two stages: boundary diffusion and intra-particle diffusion (Huang et al., 2018a). The slope and correlation coefficient of the first step were higher at both low and high concentrations (0.96 and 0.98), indicating that boundary diffusion was the main rate-limiting step for the removal of Cr(VI) by SL/PEI/SA.

3.4. Adsorption isotherm

The adsorption capacity of SL/PEI/SA for Cr(VI) was also affected by the initial concentration of the Cr(VI) solution and adsorption temperature. As shown in Fig. 5a, at the same temperature, the adsorption capacity of SL/PEI/SA for Cr(VI) increased with an increase in the Cr(VI) concentration. This was because the increase in the Cr(VI) concentration increased the driving force to overcome the mass transfer resistance of Cr(VI) between the aqueous and solid phases (Chowdhury et al., 2011). Notably, even for a low Cr(VI) concentration (300 $mg{\cdot}L^{-1}$), the adsorption capacity of SL/PEI/SA to Cr(VI) remained as high as 934.7 ± 2 $mg{\cdot}g^{-1}$, showing a strong affinity for Cr(VI) adsorption.

As the temperature increased, the adsorption capacity of SL/PEI/SA for Cr(VI) gradually increased as well. Specifically, the maximum adsorption capacities of SL/PEI/SA for Cr(VI) at 10 °C, 25 °C, and 40 °C were 1538.4 + 46 $mg{\cdot}g^{-1}$, 2016.0 + 57 $mg{\cdot}g^{-1}$, and 2209.2 + 43 $mg{\cdot}g^{-1}$, respectively, which were much higher than those of previously reported adsorbents. Notably, the maximum adsorption capacity of SL/PEI/SA at 25 °C was significantly higher than that at 10 °C, but there was no significant difference in the maximum adsorption capacity of SL/PEI/SA at 40 °C, indicating that the temperature affects the adsorption capacity of SL/PEI/SA for Cr(VI) only at a low range (10–25 ℃). When the temperature was higher, its effect on adsorption was not obvious.

To better evaluate the adsorption capacity of SL/PEI/SA for Cr(VI) and understand the adsorption mechanism between SL/PEI/SA and Cr (VI), the adsorption data obtained at the aforementioned three temperatures were fitted by Langmuir model and Freundlich model (as expressed by formulae S4 and S5). According to the correlation coefficient-fitted model (Fig. S3), the R^2 value was slightly better when fitted with the Langmuir model (0.95–0.98) than with the Freundlich model (0.94–0.98); however, both models fitted the adsorption data well, indicating that the adsorption of Cr(VI) by SL/PEI/SA was not only a single monolayer or multilayer adsorption reaction but a complex process. In addition, all the 1/n values calculated by the Freundlich model were below 1, indicating that the adsorption of Cr(VI) by SL/PEI/SA is easy (Y. Wang et al., 2020; X. Wang et al., 2020).

The maximum adsorption capacities of SL/PEI/SA for Cr(VI)

Table 1
Kinetics of Cr(VI) adsorption on SL/PEI/SA.

	Pseudo-first order model			Pseudo-second order model		
q_e^{exp}	K_1	q_e^{cal}	R^2	K_2	q_e^{cal}	R^2
($mg{\cdot}g^{-1}$)	(min^{-1})	($mg{\cdot}g^{-1}$)		($g{\cdot}mg^{-1}{\cdot}min^{-1}$)	($mg{\cdot}g^{-1}$)	
612.0	3.1×10^{-3}	198.1	0.90	6.5×10^{-5}	625.0	0.99
1509.1	4.4×10^{-3}	504.2	0.98	4.1×10^{-5}	1428.6	0.99

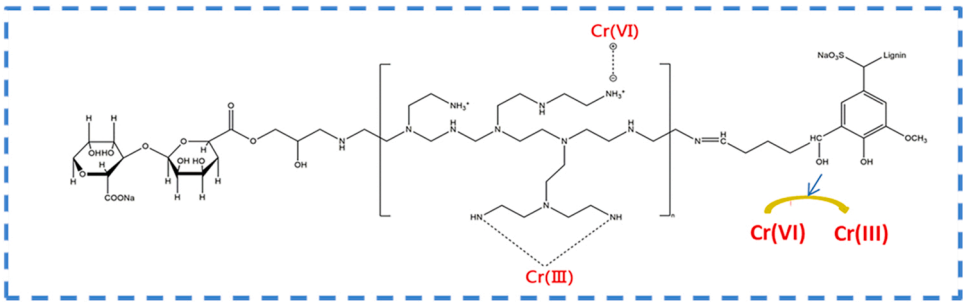

Fig. 7. Reaction mechanism of SL/PEI/SA to Cr(VI).

calculated by the Langmuir model at 10 °C, 25 °C, and 40 °C were 2000 mg·g^{-1}, 2500 mg·g^{-1}, and 3333 mg·g^{-1}, respectively (as given in Table 2). These values not only far exceeded those of the equivalent adsorbents synthesized by SA and PEI (Chen et al., 2018; Jiang et al., 2020; Qing et al., 2021; Shi et al., 2018; Yan et al., 2021), but also notably surpassed those of the majority of adsorbents reported thus far (Table S2). Therefore, the significant application potential of our proposed SL/PEI/SA gel beads for Cr (VI) removal was clearly demonstrated.

3.5. Removal rate of Cr(VI) by SL/PEI/SA

In addition to the maximum adsorption capacity, the removal rate of Cr(VI) by the adsorbent also plays a key role in its practical application. Therefore, the removal rate of Cr(VI) by SL/PEI/SA was also investigated at different concentrations (Fig. 5**b**). However, because the removal rate of Cr(VI) by adsorbent was affected by the dosage of adsorbent, the removal rate of Cr(VI) by SL/PEI/SA under different dosage was first investigated. The results are shown in Fig. S4, wherein the initial concentration of Cr(VI) solution is 200 mg·L^{-1}. As the dosage of adsorbent increases from 0.1 g·L^{-1} to 1 g·L^{-1}, the adsorption capacity of SL/PEI/SA for Cr(VI) decreased from 712.5 mg·g^{-1} to 198.7 mg·g^{-1}; however, the removal rate increased from 37 % to 100 %, indicating that the removal rate of Cr(VI) by SL/PEI/SA increases with the increase in dosage. In this study, the removal rate of Cr(VI) by SL/PEI/SA was investigated under the condition of 1 g·L^{-1} (solid-to-liquid ratio), which is currently the commonly reported solid–liquid ratio, to facilitate the comparison of the removal rate of SL/PEI/SA with other adsorbents. The removal rate of Cr(VI) with different concentrations by SL/PEI/SA is shown in Fig. 5b, wherein the initial concentrations of Cr(VI) were 50 mg·L^{-1}, 100 mg·L^{-1}, 200 mg·L^{-1}, and 300 mg·L^{-1}. Furthermore, the pH of Cr(VI) solution was 2, the removal rate of Cr(VI) by SL/PEI/SA reached 100 %, and the removal rate reached 98 % at 400 mg.L^{-1}. When the pH of Cr(VI) solution was not adjusted using acid, the removal rate of Cr(VI) by SL/PEI/SA could reach 92 %, 74 %, and 62 % at the initial concentrations of 200 mg·L^{-1}, 300 mg·L^{-1}, and 400 mg·L^{-1}. These results verified the excellent removal ability of SL/PEI/SA for Cr(VI) in water environments.

3.6. Effect of HA on the adsorption capacity of SL/PEI/SA

Dissolved organic matter (DOM) is common in industrial wastewater and its concentration can be as high as 40 mg·C·L^{-1} (Huang et al., 2020). Previous reports have shown that DOM may affect the adsorption capacity of adsorbent on Cr (VI) (Liu et al., 2009; Rouhaninezhad et al., 2020). In this study, the effect of humic acid (HA) as the main component of DOM on the adsorption effect of SL/PEI/SA for Cr(VI) was investigated at pH 2. The adsorption capacity of SL/PEI/SA for Cr(VI) without HA was 387.0 mg·g^{-1}. When HA exists, the concentration of HA increased from 5 mg·L^{-1} to 20 mg·L^{-1}, and the adsorption capacity of SL/PEI/SA increased from 387.8 + 2 mg·g^{-1} to 425.1 + 0.4 mg·g^{-1}. Although the adsorption capacity of SL/PEI/SA for Cr(VI) did not increase when the concentration of HA increased from 20 mg·L^{-1} to 50 mg·L^{-1}, it was still higher than that of SL/PEI/SA without HA. This indicates that the presence of HA promoted the adsorption affinity of SL/PEI/SA for Cr (VI) at pH 2.

Table 2
Cr(VI) adsorption data of SL/PEI/SA at different temperatures.

	Langmuir			Freundlich		
T	q_{max}	K_L	R^2	K_F	1/n	R^2
(℃)	(mg g^{-1})	(L mg^{-1})		(L mg^{-1})		
10	2000	3.0×10^{-3}	0.95	5.3	0.49	0.94
25	2500	2.4×10^{-3}	0.99	6.4	0.47	0.98
40	3333	1.7×10^{-3}	0.98	6.9	0.46	0.98

To investigate why HA promoted the Cr(VI) removal by SL/PEI/SA, the Cr concentration in the solution after adsorption was determined using ICP-OES. The results of ICP-OES showed that when the HA concentrations were 0 mg·L^{-1}, 5 mg·L^{-1}, 10 mg·L^{-1}, 15 mg·L^{-1}, 20 mg·L^{-1}, and 50 mg·L^{-1}, the Cr(III) contents in the filtrate at the adsorption equilibrium were 10.9 mg·L^{-1}, 11.0 mg·L^{-1}, 11.1 mg·L^{-1}, 11.5 mg·L^{-1}, 11.9 mg·L^{-1}, and 11·8 mg·L^{-1}, respectively (Fig. 5e, broken line). This indicates that the presence of HA promoted the reduction of Cr(VI) to Cr (III). The influence of HA on Cr(VI) adsorption by SL/PEI/SA was theorized to include the following aspects (Huang et al., 2020): (1) At the low pH (< 3.5), the phenolic hydroxyl groups of HA bound to the surface of SL/PEI/SA partially reduced Cr(VI) to Cr(III). (2) The partially reduced Cr(III) in the solution exhibited electrostatic adsorption and chemical complexation reactions with the –COOH groups of HA that were bound on the SL/PEI/SA surface.

Furthermore, the effect of HA on the adsorption capacity of SL/PEI/SA at pH 7 was studied. As shown in Fig. 5f, lower concentrations of HA (5 mg·L^{-1} and 10 mg·L^{-1}) had no effects on the adsorption capacity of SL/PEI/SA, whereas higher concentrations of HA (15 mg·L^{-1}, 20 mg·L^{-1} and 50 mg·L^{-1}) slightly inhibited the adsorption capacity of SL/PEI/SA. In addition, the Cr (III) content in the filtrate did not change significantly with the increase in HA concentrations (Fig. 5f, broken line), which proved that HA did not promote the reduction of Cr (VI) at pH 7. The reasons for the aforementioned results are that the surface charge of SL/PEI/SA is negative at pH 7, and the amount of HA adsorbed to the SL/PEI/SA surface is reduced due to electrostatic repulsion, the electron donor capacity of HA decreases with the decrease in the amount of HA adsorbed to the SL/PEI/SA surface (Huang et al., 2020). Therefore, HA could not improve the adsorption effect of SL/PEI/SA by promoting the reduction of Cr(VI) at pH 7. When the concentration of HA was higher (50 mg·L^{-1}), negatively charged HA competed with Cr(VI) for active reaction sites on the surface of SL/PEI/SA. This resulted in a slight decrease in the amount of Cr(VI) adsorbed (as shown in Fig. 5f).

3.7. Effect of coexisting ions on the adsorption capacity of SL/PEI/SA

Industrial wastewater usually contains anions coexisting with Cr (VI), such as Cl^-, NO_3^-, SO_4^{2-}, which can compete with Cr(VI) for active sites on the adsorbent and can interfere with the removal of Cr(VI) from wastewater. Fig. 5d shows the effect of coexisting anions on the adsorption capacity of SL/PEI/SA. When there was no coexisting anion, the adsorption capacity of SL/PEI/SA for Cr(VI) was 554.0 ± 6.1 mg·L^{-1}. In the presence of Cl^- and NO_3^-, as their concentration increased from 50 mg·L^{-1} to 150 mg·L^{-1}, the adsorption capacity of SL/PEI/SA decreased from 544.6 mg·L^{-1} and 521.3 mg·L^{-1} to 511.3 mg·L^{-1} and 520 mg·L^{-1}, respectively, indicating that the effects of these two anions on Cr(VI) adsorption were not significant. When SO_4^{2-} exists, the adsorption capacity of SL/PEI/SA decreases to 472.8 mg·L^{-1} with the increase in SO_4^{2-} concentration, indicating that SO_4^{2-} significantly interferes with the adsorption of Cr(VI) by SL/PEI/SA.

The various inhibitory effects of Cl^-, NO_3^-, and SO_4^{2-} on Cr(VI) adsorption are related to their valence, hydration state, and chemical structure of anions. The reason for Cl^- and NO_3^- anions to exhibit slight effects on Cr(VI) adsorption is that the affinities of Cl^- and NO_3^- through outer-sphere complexes with binding surfaces are relatively weak (Dong et al., 2018). Compared to Cl^- and NO_3^-, the coexisting SO_4^{2-} has a significant inhibitory effect on the adsorption of Cr(VI). This is because the ion energy and electrostatic adsorption of SO_4^{2-} (di-anion anion) are stronger than that of monovalent ion, which has stronger competitiveness for the positive charge sites on the surface of SL/PEI/SA, thereby weakening the adsorption of Cr(VI) (Dong et al., 2018; Huang et al., 2018b).

3.8. Thermodynamic study

The temperature dependence on the adsorption of Cr(VI) by SL/PEI/SA is associated with thermodynamic parameters (i.e., standard free energy change (ΔG^o), enthalpy change (ΔH^o), and entropy change (ΔS^o)) (Huang et al., 2018b). Here, ΔG^o is an indication of the spontaneity of the chemical reaction. The value of ΔH^o can reflect whether the adsorption reaction is an endothermic or exothermic, and the value of ΔS^o reflects the affinity of Cr(VI) for the adsorbent (Ucun et al., 2008). The thermodynamic parameters calculated are given in Table S3. Here, ΔG^o was negative, indicating that the adsorption by SL/PEI/SA was spontaneous. The value of ΔH^o was 7.5 (positive), which reflects that the adsorption of SL/PEI/SA was an endothermic reaction. Furthermore, this was supported by the increase in the adsorption capacity of SL/PEI/SA with the increase in temperature. The value of ΔS^o was 0.07 (positive value), indicating that the randomness at the solid–liquid interface increased while SL/PEI/SA adsorbed Cr(VI) (Huang et al., 2022).

3.9. Cr(VI) removal performance of SL/PEI/SA in wastewater

Strict control of hexavalent chromium emissions has become an international trend. The Chinese government stipulates that the concentration of Cr(VI) in the discharged industrial wastewater shall not exceed 0.2 mg·L^{-1}. In this study, pH of the wastewater used was 2.4, and it was composed of: SO_4^{2-} (646 mg·L^{-1}), Cl^{-1} (416 mg·L^{-1}), Cr(VI) (214 mg·L^{-1}), Na^{+} (168 mg·L^{-1}), COD (114 mg·L^{-1}), TN (61.3 mg·L^{-1}), Ni (47.6 mg·L^{-1}), Ca^{2+} (34.2 mg·L^{-1}), Cu^{2+} (19.6 mg·L^{-1}), ammonia nitrogen (15 mg·L^{-1}), Mg^{2+} (9.04 mg·L^{-1}), Fe^{3+} (3.06 mg·L^{-1}), Pb^{2+} (1.6 mg·L^{-1}), Zn^{2+} (1.34 mg·L^{-1}), TP (0.17 mg·L^{-1}), and petroleum (1.07 mg·L^{-1}). Although the composition of wastewater was extremely complex, when the ratio of SL/PEI/SA to wastewater was 1.1 g·L^{-1}, SL/PEI/SA could reduce the concentration of Cr(VI) in wastewater to 0.12 mg·L^{-1}, thereby meeting the discharge standard (< 0.2 mg·L^{-1}). This strongly suggests the substantial application potential of SL/PEI/SA for Cr(VI) removal in water environments.

To study the competitive effect of other components in wastewater, the components of wastewater treated by SL/PEI/SA were analyzed. The results showed that in addition to the reduction of Cr(VI) concentration from 214 mg·L^{-1} to 0.12 mg·L^{-1}, the concentrations of Cl^{-1} and SO_4^{2-} also decreased from 416 mg·L^{-1} and 646 mg·L^{-1} to 196 mg·L^{-1} and 421 mg·L^{-1} respectively. This indicates that Cl^{-1} and SO_4^{2-} participated in the adsorption competition with Cr(VI), which was consistent with the results in described in Section 3.7.

3.10. Regeneration capacity of SL/PEI/SA

The change in the adsorption performance of the SL/PEI/SA gel beads over 10 adsorption–desorption cycles is shown in Fig. 5**c**. After the first desorption, the adsorption capacity of the SL/PEI/SA beads in the second cycle was 84 % of its initial value. The main reason for this decrease was as follows: a small portion of SA and SL that did not participate in the crosslinking reaction dissolved in the desorption solution, resulting in the reduction of the adsorption sites on the SL/PEI/SA surface, which was verified by the blank test conducted in this study. The crosslinking reaction of PEI with SA and SL is important to maintain the stability of SL/PEI/SA under alkaline conditions (see Section 3.2). Therefore, if the amount of PEI is insufficient to crosslink with all SA and SL, the SA and SL without crosslinking reactions with PEI will be dissolved in the alkaline solution (desorption solution). Furthermore, the amount of glutaraldehyde (crosslinking agent) can affect the degree of crosslinking between PEI and SA and SL, which has been confirmed using our previous experiments. In the synthesis of SL/PEI/SA, the amounts of SL, SA, and PEI were 0.4, 0.2, and 0.2 g, respectively. The amount of the crosslinking agent (glutaraldehyde) was 0.7 mL. Therefore, the reason why small amounts of SA and SL dissolve in the alkaline solution (desorption solution) can be: 1) the amount of PEI is not sufficient, resulting in the formation of some SA and SL that cannot cross link with PEI; and 2) 0.7 mL of glutaraldehyde is not sufficient to crosslink PEI with all SA and SL.

Significantly, the adsorption capacities of the SL/PEI/SA beads during the 3rd–5th cycles were maintained at 99–93 % of its value during the 2nd cycle, indicating that after the first desorption, the remaining components on the SL/PEI/SA could remain stable in the desorption solution. From the 6th to 10th cycles, the adsorption capacity of SL/PEI/SA decreased significantly. The reason for this result is that Cr (III) adsorbed on the SL/PEI/SA surface easily precipitated under alkaline condition, and formed a very stable complex with the organic ligands of hydrogels (Song et al., 2019). As we did not use the acid desorption solution to desorb the adsorbed Cr(III) on the SL/PEI/SA surface, the amount of Cr (III) precipitated on the surface of SL/PEI/SA increased after multiple cycles of adsorption (form the first to 5th cycles). This resulted in a significant decrease in the adsorption capacity of SL/PEI/SA in the 6th cycle. In addition, during the cycles, the content of hydroxyl groups on SL/PEI/SA that provide electrons for Cr(VI) reduction was reduced, which further inhibits the adsorption of Cr (VI) (Song et al., 2019).

Compared to the excellent adsorbents that were reported, the regeneration adsorption capacity of SL/PEI/SA in the first five cycles was lower than that of several excellent adsorbents (as listed in Table S4). However, the adsorption capacity of SL/PEI/SA can still maintain 65 % at the 10th cycle, it significantly exceeded the maximum adsorption capacity of most reported adsorbents because of the ultra-high adsorption capacity of SL/PEI/SA for Cr(VI) (2015.3 mg.g^{-1}). Consequently, these results verified that SL/PEI/SA is a promising adsorbent for the removal of Cr(VI) from aqueous solutions.

3.11. Dynamic adsorption experiment

We evaluated the application potential of SL/PEI/SA in Cr(VI) solution through a column adsorption experiment (Fig. 6**a**). Specifically, when the concentration of the Cr(VI) solution was 100 mg·L^{-1} and the flow rate was 1.5 mL·min^{-1}, the breakthrough time for 1 g of SL/PEI/SA to Cr(VI) was 8140 min (Fig. 6b), and the volume of Cr(VI) solution treated was 12.2 L. Specifically, when the volume of Cr(VI) solution treated was 0.5 L, the concentration of Cr(VI) in the effluent solution treated by SL/PEI/SA was 80 μg·L^{-1}. Even when the volume of Cr(VI) solution treated was 1.5 L, the removal rate of Cr(VI) by SL/PEI/SA could reach 99 %.

To evaluate the ability of SL/PEI/SA to treat real wastewater, we studied the ability of SL/PEI/SA to remove Cr(VI) from secondary electroplating wastewater in column adsorption experiment. Secondary electroplating wastewater is the wastewater that has been treated by the factory but has not yet reached the discharge standard. The content of Cr (VI) in the secondary electroplating wastewater was 2.4 mg·L^{-1}, but it was still higher than the wastewater discharge standard stipulated by China (< 0.2 mg·L^{-1}). Furthermore, the wastewater contained other high concentration complex components, such as SO_4^{2-} (1250 mg·L^{-1}), Na^{+} (542 mg·L^{-1}), Cl^{-1} (432 mg·L^{-1}), Ca^{2+} (302 mg·L^{-1}), COD (36 mg·L^{-1}), TN (27.9 mg·L^{-1}), Mg^{2+} (9 mg·L^{-1}), ammonia nitrogen (3.5 mg·L^{-1}), fluoride (1.12 mg·L^{-1}), petroleum (1.07 mg·L^{-1}), aluminium (0.1 mg·L^{-1}), Ni (44.7 μg·L^{-1}), TP (20 μg·L^{-1}), Cu^{2+} (9.8 μg·L^{-1}), and Zn^{2+} (6.28 μg·L^{-1}). The results showed that that 1 g of SL/PEI/SA could treat 8.1 L of secondary electroplating wastewater to meet the discharge standard (< 0.2 mg·L^{-1}) when the flow rate was 0.5 mL·min^{-1}. These results demonstrate the applicability of SL/PEI/SA to real-world wastewater treatment.

3.12. Adsorption mechanism of SL/PEI/SA for Cr(VI)

Based on the FTIR and XPS results, the main Cr(VI) adsorption mechanism by SL/PEI/SA was deduced and is described below (Fig. 7b):

(1) Under acidic conditions, the amine (–NH–/– NH_2) on the surface of SL/PEI/SA became protonated and adsorbed the negatively charged Cr (VI) species through electrostatic adsorption. (2) The abundant –OH groups on the SL/PEI/SA surface acted as an electron donor group, contributing to the reduction of Cr(VI) to Cr(III). (3) Amine, imine, and sulfonic acid groups on SL/PEI/SA reacted with the positively charged Cr(III) species and facilitated their loading onto the SL/PEI/SA surface, through the following specific reactions (Q. Wang et al., 2021; X. Wang et al., 2021):

$$R - NH_3^+ + HCrO_4^- \rightarrow R - NH_3^+ \cdots HCrO_4^-, \quad (1)$$

$$R - NH_3^+ + Cr_2O_7^{2-} \rightarrow R - NH_3^+ \cdots Cr_2O_7^{2-}, \quad (2)$$

$$3(\mathrm{R-OH}) + HCrO_4^- + 4H^+ \rightarrow 3(R - O) + Cr^{3+} + 4H_2O, \quad (3)$$

$$R - NH_2 + Cr^{3+} \rightarrow R - NH_2 \cdots Cr^{3+}, \quad (4)$$

$$R - SO_3^- + Cr^{3+} \rightarrow R - SO_3^- \cdots Cr^{3+}. \quad (5)$$

The SEM and BET results revealed that the SL/PEI/SA beads were composed of 3D porous network structures, which provided a channel for Cr(VI) species to move rapidly from the surface of SL/PEI/SA to the interior, facilitating full contact with a large number of functional groups in SL/PEI/SA in the process. Owing to this, the SL/PEI/SA beads could rapidly and efficiently adsorb Cr(VI).

4. Conclusions

In this study, SL and PEI-modified alginate gel beads were synthesized through a simple cross-linking strategy. The SL/PEI/SA gel beads could effectively separate from water and showed a strong affinity for Cr (VI) species, rapidly removing them from the solution and demonstrating an ultra-high maximum adsorption capacity of 2500 $mg{\cdot}g^{-1}$ at 25 ℃. Furthermore, the SL/PEI/SA gel beads showed excellent anti-interference features during the Cr(VI) adsorption process. In the continuous dynamic adsorption experiment, 1 g of SL/PEI/SA could treat 8.1 L of secondary electroplating wastewater and was able to meet the discharge concentration standard stipulated by China (< 0.2 $mg{\cdot}L^{-1}$). These results demonstrate the effectiveness of SL/PEI/SA gel beads for removing Cr (VI) from water, thereby mitigating risks associated with pollution.

CRediT authorship contribution statement

Yimin Huang: Conceptualization, Investigation, Data curation, Funding Acquisition, Visualization, Roles/Writing – original draft. **Bing Wang:** Data discussion, Writing – review & editing. **Jiapei Lv:** Investigation, Data discussion. **Yingnan He:** Validation, Data discussion. **Hucai Zhang:** Visualization, Investigation, Data discussion. **Wenyan Li:** Investigation, Data discussion. **Yongtao Li:** Resources, Data discussion. **Thomas Wågberg:** Data discussion, Draft check. **Guangzhi Hu:** Data discussion, Writing – review & editing, Project administration, Funding acquisition, Supervision.

Environmental Implication

Hexavalent chromium in industrial wastewater can pose a serious threat to the environment and human health. In this study, gel beads synthesized by crosslinking with renewable alginate, lignosulfonate produced by industrial by-products, and polyethyleneimine are shown to efficiently reduce the concentration of Cr(VI) in electroplating wastewater such that it meets the national permitted emission standard. This provides novel technical support for Cr(VI) removal from wastewater and can simultaneously achieve the goals of resource utilization and environmental protection.

Declaration of Competing Interest

The authors declare that they have no known competing financial interests or personal relationships that could have appeared to influence the work reported in this paper.

Acknowledgment

This work was financially supported by the Special Project for Social Development of Yunnan Province (202103AC100001), Postdoctoral Research Projects Funding of Yunnan Province (C615300504015), the Double Tops Joint Fund of the Yunnan Science and Technology Bureau and Yunnan University (2019FY003025), and Double First Class University Plan (C176220100042). The authors thank the Advanced Analysis and Measurement Center of Yunnan University for the sample testing service.

Appendix A. Supporting information

Supplementary data associated with this article can be found in the online version at doi:10.1016/j.jhazmat.2022.129270.

References

Bao, S., Yang, W., Wang, Y., Yu, Y., Sun, Y., Li, K., 2020. PEI grafted amino-functionalized graphene oxide nanosheets for ultrafast and high selectivity removal of Cr(VI) from aqueous solutions by adsorption combined with reduction: behaviors and mechanisms. Chem. Eng. J. 399, 125762 https://doi.org/10.1016/j.cej.2020.125762.

Boparai, H.K., Joseph, M., O'Carroll, D.M., 2011. Kinetics and thermodynamics of cadmium ion removal by adsorption onto nano zerovalent iron particles. J. Hazard. Mater. 186 (1), 458–465. https://doi.org/10.1016/j.jhazmat.2010.11.029.

Chen, J.H., Liu, Q.L., Hu, S.R., Ni, J.C., He, Y.S., 2011. Adsorption mechanism of Cu(II) ions from aqueous solution by glutaraldehyde crosslinked humic acid-immobilized sodium alginate porous membrane adsorbent. Chem. Eng. J. 173 (2), 511–519. https://doi.org/10.1016/j.cej.2011.08.023.

Chen, S., Wang, J., Wu, Z., Deng, Q., Tu, W., Dai, G., Zeng, Z., Deng, S., 2018. Enhanced Cr(VI) removal by polyethylenimine- and phosphorus-codoped hierarchical porous carbons. J. Colloid Interface Sci. 523, 110–120. https://doi.org/10.1016/j.jcis.2018.03.057.

Chen, Z., Li, Y., Guo, M., Xu, F., Wang, P., Du, Y., Na, P., 2016. One-pot synthesis of Mn-doped TiO2 grown on graphene and the mechanism for removal of Cr(VI) and Cr (III). J. Hazard. Mater. 310, 188–198. https://doi.org/10.1016/j.jhazmat.2016.02.034.

Chowdhury, S., Mishra, R., Saha, P., Kushwaha, P., 2011. Adsorption thermodynamics, kinetics and isosteric heat of adsorption of malachite green onto chemically modified rice husk. Desalination 265 (1), 159–168. https://doi.org/10.1016/j.desal.2010.07.047.

Dong, L., Liang, J., Li, Y., Hunang, S., Wei, Y., Bai, X., Jin, Z., Zhang, M., Qu, J., 2018. Effect of coexisting ions on Cr(VI) adsorption onto surfactant modified Auricularia auricula spent substrate in aqueous solution. Ecotoxicol. Environ. Saf. 166, 390–400. https://doi.org/10.1016/j.ecoenv.2018.09.097.

Fang, L., Ding, L., Ren, W., Hu, H., Huang, Y., Shao, P., Yang, L., Shi, H., Ren, Z., Han, K., Luo, X., 2021. High exposure effect of the adsorption site significantly enhanced the adsorption capacity and removal rate: a case of adsorption of hexavalent chromium by quaternary ammonium polymers (QAPs). J. Hazard. Mater. 416, 125829 https://doi.org/10.1016/j.jhazmat.2021.125829.

Feng, Y., Wang, H., Xu, J., Du, X., Cheng, X., Du, Z., Wang, H., 2021. Fabrication of MXene/PEI functionalized sodium alginate aerogel and its excellent adsorption behavior for Cr(VI) and Congo Red from aqueous solution. J. Hazard. Mater. 416, 125777 https://doi.org/10.1016/j.jhazmat.2021.125777.

Gao, S., Luo, T., Zhou, Q., Luo, W., Li, H., Jing, L., 2018. Surface sodium lignosulphonate-immobilized sawdust particle as an efficient adsorbent for capturing Hg2+ from aqueous solution. J. Colloid Interface Sci. 517, 9–17. https://doi.org/10.1016/j.jcis.2017.12.008.

Guo, D.-M., An, Q.-D., Xiao, Z.-Y., Zhai, S.-R., Yang, D.-J., 2018. Efficient removal of Pb (II), Cr(VI) and organic dyes by polydopamine modified chitosan aerogels. Carbohydr. Polym. 202, 306–314. https://doi.org/10.1016/j.carbpol.2018.08.140.

Huang, Y., He, Y., Zhang, H., Wang, H., Li, W., Li, Y., Xu, J., Wang, B., Hu, G., 2022. Selective adsorption behavior and mechanism of phosphate in water by different lanthanum modified biochar. J. Environ. Chem. Eng. 10 (3), 107476 https://doi.org/10.1016/j.jece.2022.107476.

Huang, Y., Lee, X., Grattieri, M., Macazo, F.C., Cai, R., Minteer, S.D., 2018a. A sustainable adsorbent for phosphate removal: modifying multi-walled carbon nanotubes with chitosan. J. Mater. Sci. 53 (17), 12641–12649. https://doi.org/10.1007/s10853-018-2494-y.

Huang, Y., Lee, X., Macazo, F.C., Grattieri, M., Cai, R., Minteer, S.D., 2018b. Fast and efficient removal of chromium (VI) anionic species by a reusable chitosan-modified

multi-walled carbon nanotube composite. Chem. Eng. J. 339, 259–267. https://doi.org/10.1016/j.cej.2018.01.133.
Huang, Y., Song, K., Luo, W., Yang, J., 2020. Adsorption and reduction of Cr(VI) by hydroxylated multiwalled carbon nanotubes: effects of humic acid and surfactants. Environ. Sci. Pollut. Res. 27 (11), 12746–12754. https://doi.org/10.1007/s11356-020-07682-y.
Huang, Y., Wu, H., Shao, T., Zhao, X., Peng, H., Gong, Y., Wan, H., 2018c. Enhanced copper adsorption by DTPA-chitosan/alginate composite beads: Mechanism and application in simulated electroplating wastewater. Chem. Eng. J. 339, 322–333. https://doi.org/10.1016/j.cej.2018.01.071.
Jiang, H., Yang, Y., Lin, Z., Zhao, B., Wang, J., Xie, J., Zhang, A., 2020. Preparation of a novel bio-adsorbent of sodium alginate grafted polyacrylamide/graphene oxide hydrogel for the adsorption of heavy metal ion. Sci. Total Environ. 744, 140653 https://doi.org/10.1016/j.scitotenv.2020.140653.
Jiao, C., Li, T., Wang, J., Wang, H., Zhang, X., Han, X., Du, Z., Shang, Y., Chen, Y., 2020. Efficient removal of dyes from aqueous solution by a porous sodium alginate/gelatin/graphene oxide triple-network composite aerogel. J. Polym. Environ. 28 (5), 1492–1502. https://doi.org/10.1007/s10924-020-01702-1.
Lian, G., Wang, B., Lee, X., Li, L., Liu, T., Lyu, W., 2019. Enhanced removal of hexavalent chromium by engineered biochar composite fabricated from phosphogypsum and distillers grains. Sci. Total Environ. 697, 134119 https://doi.org/10.1016/j.scitotenv.2019.134119.
Liang, H., Song, B., Peng, P., Jiao, G., Yan, X., She, D., 2019. Preparation of three-dimensional honeycomb carbon materials and their adsorption of Cr(VI). Chem. Eng. J. 367, 9–16. https://doi.org/10.1016/j.cej.2019.02.121.
Liao, T., Huang, P., Song, H., Guo, J., Fu, X., Yu, X., Peng, L., Han, B., Zhu, Y., Zhang, Y., 2020. La(OH)3-modified magnetic sodium carboxymethyl cellulose for sequential removal of pollutants: adsorption of phosphate and subsequent photocatalytical reduction of Cr(VI). Environ. Sci. Pollut. Res. 27 (32), 40346–40354. https://doi.org/10.1007/s11356-020-09904-9.
Liu, Q., Tang, J., Li, X., Lin, Q., Xiao, R., Zhang, M., Yin, G., Zhou, Y., 2020. Effect of lignosulfonate on the adsorption performance of hematite for Cd(II). Sci. Total Environ. 738, 139952 https://doi.org/10.1016/j.scitotenv.2020.139952.
Liu, S., Gao, J., Zhang, L., Yang, Y., Liu, X., 2021. Diethylenetriaminepentaacetic acid–thiourea-modified magnetic chitosan for adsorption of hexavalent chromium from aqueous solutions. Carbohydr. Polym. 274, 118555 https://doi.org/10.1016/j.carbpol.2021.118555.
Liu, T., Rao, P., Lo, I.M.C., 2009. Influences of humic acid, bicarbonate and calcium on Cr (VI) reductive removal by zero-valent iron. Sci. Total Environ. 407 (10), 3407–3414. https://doi.org/10.1016/j.scitotenv.2009.01.043.
Liu, W., Jin, L., Xu, J., Liu, J., Li, Y., Zhou, P., Wang, C., Dahlgren, R.A., Wang, X., 2019. Insight into pH dependent Cr(VI) removal with magnetic Fe_3S_4. Chem. Eng. J. 359, 564–571. https://doi.org/10.1016/j.cej.2018.11.192.
Nasseh, N., Khosravi, R., Rumman, G.A., Ghadirian, M., Eslami, H., Khoshnamvand, M., Al-Musawi, T.J., Khosravi, A., 2021. Adsorption of Cr(VI) ions onto powdered activated carbon synthesized from Peganum harmala seeds by ultrasonic waves activation. Environ. Technol. Innov. 21, 101277 https://doi.org/10.1016/j.eti.2020.101277.
Niu, C., Zhang, N., Hu, C., Zhang, C., Zhang, H., Xing, Y., 2021. Preparation of a novel citric acid-crosslinked Zn-MOF/chitosan composite and application in adsorption of chromium(VI) and methyl orange from aqueous solution. Carbohydr. Polym. 258, 117644 https://doi.org/10.1016/j.carbpol.2021.117644.
Qing, Z., Wang, L., Liu, X., Song, Z., Qian, F., Song, Y., 2021. Simply synthesized sodium alginate/zirconium hydrogel as adsorbent for phosphate adsorption from aqueous solution: Performance and mechanisms. Chemosphere, 133103. https://doi.org/10.1016/j.chemosphere.2021.133103.
Rouhaninezhad, A.A., Hojati, S., Masir, M.N., 2020. Adsorption of Cr (VI) onto micro- and nanoparticles of palygorskite in aqueous solutions: Effects of pH and humic acid. Ecotoxicol. Environ. Saf. 206, 111247 https://doi.org/10.1016/j.ecoenv.2020.111247.
Shi, Y., Zhang, T., Ren, H., Kruse, A., Cui, R., 2018. Polyethylene imine modified hydrochar adsorption for chromium (VI) and nickel (II) removal from aqueous solution. Bioresour. Technol. 247, 370–379. https://doi.org/10.1016/j.biortech.2017.09.107.
Song, L., Liu, F., Zhu, C., Li, A., 2019. Facile one-step fabrication of carboxymethyl cellulose based hydrogel for highly efficient removal of Cr(VI) under mild acidic condition. Chem. Eng. J. 369, 641–651. https://doi.org/10.1016/j.cej.2019.03.126.
Su, Q., Khan, A.A., Su, Z., Tian, C., Li, X., Gu, J., Zhang, T., Ahmad, R., Su, X., Lin, Z., 2021. Nov. Nitrogen-doped KFeS2/C. Compos. Effic. Remov. Cr(vi). Environ. Sci.: Nano, 8, 4, pp. 1057–1066 doi: 10.1039/D0EN01283A.
Sun, X., Chen, J.H., Su, Z., Huang, Y., Dong, X., 2016. Highly effective removal of Cu(II) by a novel 3-aminopropyltriethoxysilane functionalized polyethyleneimine/sodium alginate porous membrane adsorbent. Chem. Eng. J. 290, 1–11. https://doi.org/10.1016/j.cej.2015.12.106.
Sun, Y., Liu, X., Lv, X., Wang, T., Xue, B., 2021. Synthesis of novel lignosulfonate-modified graphene hydrogel for ultrahigh adsorption capacity of Cr(VI) from wastewater. J. Clean. Prod. 295, 126406 https://doi.org/10.1016/j.jclepro.2021.126406.
Ucun, H., Bayhan, Y.K., Kaya, Y., 2008. Kinetic and thermodynamic studies of the biosorption of Cr(VI) by Pinus sylvestris Linn. J. Hazard. Mater. 153 (1), 52–59. https://doi.org/10.1016/j.jhazmat.2007.08.018.
Wang, B., Wan, Y., Zheng, Y., Lee, X., Liu, T., Yu, Z., Huang, J., Ok, Y.S., Chen, J., Gao, B., 2019. Alginate-based composites for environmental applications: a critical review. Crit. Rev. Environ. Sci. Technol. 49 (4), 318–356. https://doi.org/10.1080/10643389.2018.1547621.
Wang, G., Hua, Y., Su, X., Komarneni, S., Ma, S., Wang, Y., 2016. Cr(VI) adsorption by montmorillonite nanocomposites. Appl. Clay Sci. 124–125, 111–118. https://doi.org/10.1016/j.clay.2016.02.008.
Wang, Q., Tian, Y., Kong, L., Zhang, J., Zuo, W., Li, Y., Cai, G., 2021. A novel 3D superelastic polyethyleneimine functionalized chitosan aerogels for selective removal of Cr(VI) from aqueous solution: performance and mechanisms. Chem. Eng. J. 425, 131722 https://doi.org/10.1016/j.cej.2021.131722.
Wang, X., Li, X., Peng, L., Han, S., Hao, C., Jiang, C., Wang, H., Fan, X., 2021. Effective removal of heavy metals from water using porous lignin-based adsorbents. Chemosphere 279, 130504. https://doi.org/10.1016/j.chemosphere.2021.130504.
Wang, X., Xu, J., Liu, J., Liu, J., Xia, F., Wang, C., Dahlgren, R.A., Liu, W., 2020. Mechanism of Cr(VI) removal by magnetic greigite/biochar composites. Sci. Total Environ. 700, 134414 https://doi.org/10.1016/j.scitotenv.2019.134414.
Wang, Y., Yang, Q., Chen, J., Yang, J., Zhang, Y., Chen, Y., Li, X., Du, W., Liang, A., Ho, S.-H., Chang, J.-S., 2020. Adsorption behavior of Cr(VI) by magnetically modified Enteromorpha prolifera based biochar and the toxicity analysis. J. Hazard. Mater. 395, 122658 https://doi.org/10.1016/j.jhazmat.2020.122658.
Xie, M.-Y., Wang, J., Wu, Q.-Y., 2020. Nanofiltration membranes via layer-by-layer assembly and cross-linking of polyethyleneimine/sodium lignosulfonate for heavy metal removal. Chin. J. Polym. Sci. 38 (9), 965–972. https://doi.org/10.1007/s10118-020-2422-x.
Xue, J., Cai, J., Aikelaimu, A., Li, Y., 2022. Removal of Cr (III) from aqueous solutions by carbon lignin-based composite. Sep. Sci. Technol. 57 (4), 523–531. https://doi.org/10.1080/01496395.2021.1920980.
Yan, Y.-Z., An, Q.-D., Xiao, Z.-Y., Zhai, S.-R., Zhai, B., Shi, Z., 2017. Interior multi-cavity/surface engineering of alginate hydrogels with polyethylenimine for highly efficient chromium removal in batch and continuous aqueous systems. J. Mater. Chem. A 5 (32), 17073–17087. https://doi.org/10.1039/C7TA05679F.
Yan, Y.-Z., Nagappan, S., Yoo, J.-M., Nechikkattu, R., Park, S.S., Ha, C.-S., 2021. Polyethyleneimine-grafted polysilsesquioxane hollow spheres for the highly efficient removal of anionic dyes and selective adsorption of Cr(VI). J. Environ. Chem. Eng. 9 (2), 104814 https://doi.org/10.1016/j.jece.2020.104814.
Yan, Y., An, Q., Xiao, Z., Zheng, W., Zhai, S., 2017. Flexible core-shell/bead-like alginate@PEI with exceptional adsorption capacity, recycling performance toward batch and column sorption of Cr(VI). Chem. Eng. J. 313, 475–486. https://doi.org/10.1016/j.cej.2016.12.099.
Yang, H.-R., Yang, C., Li, S.-S., Shan, X.-C., Song, G.-L., An, Q.-D., Zhai, S.-R., Xiao, Z.-Y., 2022. Site-imprinted hollow composites with integrated functions for ultra-efficient capture of hexavalent chromium from water. Sep. Purif. Technol. 284, 120240 https://doi.org/10.1016/j.seppur.2021.120240.
Yang, K., Xing, J., Xu, P., Chang, J., Zhang, Q., Usman, K.M., 2020. Act. Carbon Micro Sodium Lignosulfonate Cr(VI) Adsorpt. Eval. Wastewater Treat., 12, 1, p. 236 doi: 10.3390/polym12010236.
Yang, Q., Wang, H., Li, F., Dang, Z., Zhang, L., 2021. Rapid and efficient removal of Cr (vi) by a core–shell magnetic mesoporous polydopamine nanocomposite: roles of the mesoporous structure and redox-active functional groups. J. Mater. Chem. A 9 (22), 13306–13319. https://doi.org/10.1039/D1TA02475B.
Zhang, L., Song, F., Wang, S., Wang, H., Yang, W., Li, Y., 2020. Efficient removal of hexavalent chromium and congo red by graphene oxide/silica nanosheets with multistage pores. J. Chem. Eng. Data 65 (9), 4354–4368. https://doi.org/10.1021/acs.jced.0c00006.
Zhang, N., Cheng, N., Liu, Q., 2021. Functionalized biomass carbon-based adsorbent for simultaneous removal of Pb^{2+} and MB in wastewater. Materials 14 (13), 3537. https://doi.org/10.3390/ma14133537.
Zhang, W., Wang, H., Hu, X., Feng, H., Xiong, W., Guo, W., Zhou, J., Mosa, A., Peng, Y., 2019. Multicavity triethylenetetramine-chitosan/alginate composite beads for enhanced Cr(VI) removal. J. Clean. Prod. 231, 733–745. https://doi.org/10.1016/j.jclepro.2019.05.219.
Zhang, X., Lei, Y., Yuan, Y., Gao, J., Jiang, Y., Xu, Z., Zhao, S., 2018. Enhanced removal performance of Cr(VI) by the core-shell zeolites/layered double hydroxides (LDHs) synthesized from different metal compounds in constructed rapid infiltration systems. Environ. Sci. Pollut. Res. 25 (10), 9759–9770. https://doi.org/10.1007/s11356-018-1303-0.
Zhang, X., Sun, F., He, J., Xu, H., Cui, F., Wang, W., 2017. Robust phosphate capture over inorganic adsorbents derived from lanthanum metal organic frameworks. Chem. Eng. J. 326, 1086–1094. https://doi.org/10.1016/j.cej.2017.06.052.
Zhao, C., Hu, L., Zhang, C., Wang, S., Wang, X., Huo, Z., 2021. Preparation of biochar-interpenetrated iron-alginate hydrogel as a pH-independent sorbent for removal of Cr(VI) and Pb(II). Environ. Pollut. 287, 117303 https://doi.org/10.1016/j.envpol.2021.117303.
Zhao, N., Zhao, C., Lv, Y., Zhang, W., Du, Y., Hao, Z., Zhang, J., 2017. Adsorption and coadsorption mechanisms of Cr(VI) and organic contaminants on H3PO4 treated biochar. Chemosphere 186, 422–429. https://doi.org/10.1016/j.chemosphere.2017.08.016.